Commun. Comput. Phys.
doi: 10.4208/cicp.411011.310112s

Vol. **13**, No. 3, pp. 725-740
March 2013

A Study of Fluid Interfaces and Moving Contact Lines Using the Lattice Boltzmann Method

S. Srivastava[1,2,*], P. Perlekar[1,2], L. Biferale[3], M. Sbragaglia[3], J. H. M. ten Thije Boonkkamp[2] and F. Toschi[1,2]

[1] *Department of Applied Physics, Eindhoven University of Technology, PO Box 513, 5600 MB Eindhoven, The Netherlands.*
[2] *Department of Mathematics and Computer Science, Eindhoven University of Technology, PO Box 513, 5600 MB Eindhoven, The Netherlands.*
[3] *Department of Physics and INFN, University of Rome Tor Vergata, Via della Ricerca Scientifica 1, 00133 Rome, Italy.*

Received 31 October 2011; Accepted (in revised version) 31 January 2012

Available online 29 August 2012

Abstract. We study the static and dynamical behavior of the contact line between two fluids and a solid plate by means of the Lattice Boltzmann method (LBM). The different fluid phases and their contact with the plate are simulated by means of standard Shan-Chen models. We investigate different regimes and compare the multicomponent vs. the multiphase LBM models near the contact line. A static interface profile is attained with the multiphase model just by balancing the hydrostatic pressure (due to gravity) with a pressure jump at the bottom. In order to study the same problem with the multicomponent case we propose and validate an idea of a body force acting only on one of the two fluid components. In order to reproduce results matching an infinite bath, boundary conditions at the bath side play a key role. We quantitatively compare open and wall boundary conditions and study their influence on the shape of the meniscus against static and lubrication theory solution.

PACS: 47.55.np, 47.55.N-, 47.11.-j

Key words: Lattice-Boltzmann, multiphase flow, multicomponent flow, plunging plate problem, Landau-Levich.

1 Introduction

The motion of the contact line, the common borderline between a solid, a liquid, and its equilibrium vapor, is key to several important applications like coating, painting or

*Corresponding author. *Email addresses:* s.srivastava@tue.nl (S. Srivastava), pperlekar@gmail.com (P. Perlekar), biferale@roma2.infn.it (L. Biferale), sbragaglia@gmail.com (M. Sbragaglia), j.h.m.tenthijeboonkkamp@tue.nl (J. H. M. ten Thije Boonkkamp), f.toschi@tue.nl (F. Toschi)

oil recovery [1–3]. The dynamics of the contact line has stimulated theoretical studies and experimental investigations [4–9]. The dynamics is controlled by a rather subtle competition between the interfacial interactions amongst three phases, the dissipation in the fluid, and the geometrical or chemical patterning and irregularities of the surface. The first fundamental steps in the field are due to Landau and Levich [10] and to Derjaguin [11], who studied the problem of liquid film coating on a perfectly wetting substrate; this problem is referred to as the "LLD problem" hereafter. In the case of perfect wetting, one observes a film deposition whose thickness is controlled by the balance between viscous forces and surface tension. The solution of the LLD problem is an example of matched asymptotic between the static capillary meniscus and the liquid film (LLD film). It is well known that in a continuum description the viscous forces would diverge at the contact line [12], a problem commonly referred to as the "viscous singularity". In nature the viscous singularity is resolved by the presence of some microscopic cutoff scale, l_s, (e.g. the size of a liquid molecule) while in numerical approaches a cutoff is also invariably introduced, e.g. the size of the discretization mesh. Far from the contact line, viscous forces are negligible and the shape of the static capillary meniscus is set by the balance between gravity and surface tension.

The problem of liquid film entrainment was further investigated by de Gennes [13] for the case of partial wetting. When the liquid partially wets the plate with a non-vanishing dynamic contact angle, a steady state is achieved only for plate velocities smaller than a certain critical value. More recently it was shown that partial wetting substrates allow for the existence of a second admissible solution for the thickness of the film [8] and it was shown experimentally that in the case of non-wetting fluids a remarkable ridge-like structure is produced during the entrainment process [9]. The solution of the LLD problem has also been generalized to non-Newtonian "power law" fluids by Tallmadge [14], plastic-viscous fluids by Deryaguin and Levi [15], to include the effects of inertia by de Ryck and Quere [16], as well as the effects of Marangoni stresses by Ramdane and Quere [17].

Another case of interest is when the solid plate is plunged into the bath instead of being pulled; in the present manuscript this problem is referred to as plunging plate problem. When pulling the plate a liquid film entrainment is easily attained even at small velocities however, for case of a plunging plate this requires considerably higher velocities [18].

In the present manuscript we show numerical simulations based on the multiphase and multicomponent versions of the Lattice Boltzmann method to investigate its applicability to study the dynamics of the three phase contact line. Further, we quantitative investigate and discuss the role of boundary conditions. In Fig. 1 we report the schematic of the setup that we consider. The fluids with dynamic viscosities $\mu_1 = \rho_1 \nu_1$ and $\mu_2 = \rho_2 \nu_2$ ($\mu_2 \leq \mu_1$ and we define $R = \mu_2/\mu_1$) are separated by an interface. At the top and at the bottom boundaries we mimic an infinite bath by imposing "flux" boundary conditions (described in Section 4). The flux boundary conditions are used to sustain the hydrostatic pressure of the liquid column in the domain. At the left boundary we impose a no-slip

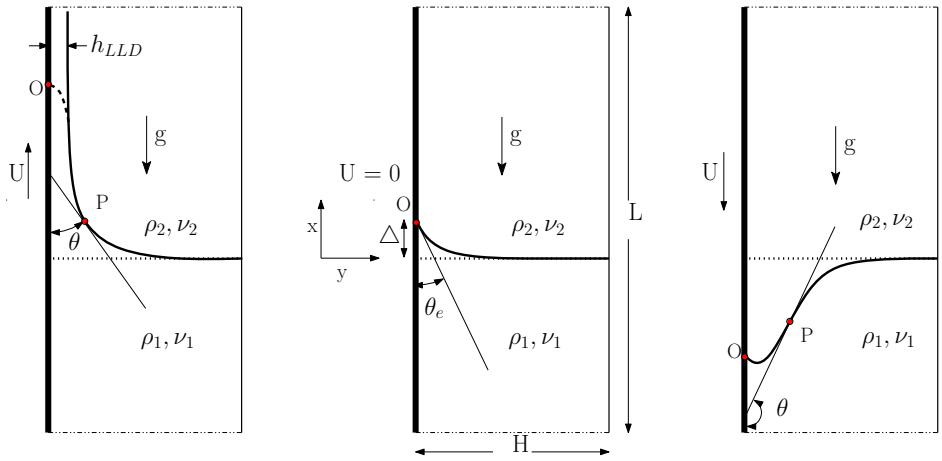

Figure 1: A schematic view of the LLD problem (left panel), interface shape for the static case (middle panel), and the plunging plate problem (right panel). At top and bottom boundaries we are using flux boundary condition. At right boundary we impose a no-slip neutral wetting wall or open boundary to mimic the infinite bath.

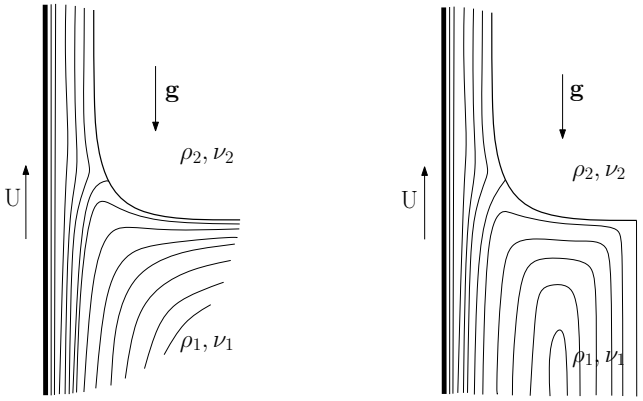

Figure 2: Schematic of the streamlines when a solid plate is vertically pulled out from a liquid bath of density ρ_1 and kinematic viscosity ν_1, into a liquid of density ρ_2 and kinematic viscosity ν_2. (Left panel) Figure shows case of an infinite bath (LLD problem), and (Right panel) the case of a fictions wall placed in the simulation instead of the infinite bath. The latter resembles closely the Bretherton problem.

wetting wall which moves with velocity U: this corresponds to the LLD problem for $U>0$, and to the plunging plate problem for $U<0$. At the right boundary we use either an infinite bath or a no-slip static wall with neutral wetting.

The infinite bath at the right boundary maps the setup to the LLD problem whereas a no-slip, neutral wetting, right boundary maps the setup onto a problem similar to the Bretherton problem [19]. The fundamental geometrical difference between the Bretherton and the LLD problems, a channel instead of a semi-infinite bath, has important implications on the flow topology, with one stagnation point for the LLD case versus two for the Bretherton problem (see Fig. 2).

The manuscript is organized as follows: in Section 2 we provide theoretical background on the problem, in Section 3 we discuss the numerical methods and the boundary conditions employed, in Section 4 results are presented and discussed while in Section 5 conclusions are drawn.

2 Theoretical background

In this section we discuss the theoretical background for interface shape with a static and a moving plate. In the first part we present the interface profile for a static plate ($U=0$) and later we show a lubrication theory based model for the moving plate problem ($U\neq 0$).

When a smooth solid plate comes in contract with the interface between two fluids, the interface close to the plate deforms due to relative interaction strength between the three phases. The condition of mechanical equilibrium (absence of forces) at the contact line is translated into the following Young equation [20]:

$$\gamma_{w2}=\gamma_{w1}+\gamma_{21}\cos(\theta_e),$$

where γ_{w2} is the surface tension between fluid 2 and plate, γ_{w1} is the surface tension between fluid 1 and plate, θ_e is the equilibrium contact angle, and γ_{21} is the surface tension between fluid 1 and 2. The equilibrium contact angle $\theta_e=0$ corresponds to perfect wetting, while $\theta_e=\pi$ corresponds to perfect dewetting. When a partial wetting solid plate ($0<\theta_e<\pi$) is put in contact with the surface of a liquid, the capillary force determines the meniscus shape close to the contact line. The equilibrium interface profile $y=h(x)$ of the meniscus (see Fig. 1 (middle panel)) can be derived using Laplace's law. An explicit relation for profile $h(x)$ and θ_e is given by [21]:

$$h(x)=l_c\text{arcosh}\left(\frac{2l_c}{x}\right)-2l_c\left(1-\left(\frac{x}{2l_c}\right)^2\right)^{1/2}+h_0, \tag{2.1}$$

with

$$h_0=-l_c\text{arcosh}\left(2/(1-\sin\theta_e)\right)^{1/2}+l_c\left(2(1+\sin\theta_e)\right)^{1/2}, \tag{2.2}$$

the capillary length $l_c=\sqrt{\gamma_{21}/(\rho_1 g)}$ and θ_e the equilibrium contact angle. The rise of the meniscus with respect to the flat interface, Δ, (see Fig. 1) can be obtained from the solution of the equation $h(\Delta)=0$. When the wall is moving, with constant velocity, the force balance is altered and the position of the contact line is displaced with respect to the static one Eq. (2.1).

2.1 The Landau-Levich-Derjaguin problem

The problem of a plate pulled out of a liquid bath has been studied by Landau and Levich [10] and Derjaguin [11] for the case of perfect wetting. In this case a liquid film of

thickness h_{LLD} is formed:

$$h_{LLD} = 0.946 l_c Ca^{2/3},$$

where $Ca = U\mu_1/\gamma_{21}$ is the capillary number and U is the magnitude of the plate velocity. This expression is however only valid at small capillary number $(Ca \ll 1)$. From the above expression one can see that a film is always entrained, unless its width becomes smaller than molecular sizes, in that case the film deposition is stopped. For the case of partial wetting, the scenario is different and there is a critical value of the capillary number, Ca_c, below which no film deposition happens and the meniscus remains static (dry wetting). The picture is qualitatively similar for the case of a plate pulled out of a liquid bath or plunged into the bath. The asymmetry between the two cases is due to the viscosity contrast R, for the LLD problem $R > 1$ whereas for the plunging plate problem $R < 1$.

2.1.1 Lubrication theory approximation

Recently an extension of the classical lubrication theory [22,23] was proposed to describe the shape of the liquid-vapor interface under moving wall conditions [24]. A crucial assumption there was that the Reynolds number, $Re \ll 1$, so that the flow in both fluid components can be obtained from Stokes' equation. The results shown for lubrication theory model in this manuscript are obtained from [24]. The viscous singularity at the moving contact line in the lubrication model is removed by using a slip length parameter, l_s, which is independent of the mechanism of the contact line motion. The interface profile obtained from the lubrication model depends on the viscosity ratio,R, on the capillary number, Ca and on the equilibrium contact angle, θ_e. Thus the steady state interface profile obtained from the lubrication model and the multicomponent or multiphase LBM models should be comparable, as long as the viscosity ratio, capillary number and the equilibrium contact angle are the same.

3 The Lattice Boltzmann method

In this section we present the details of the numerical algorithms based Lattice Boltzmann method. We employ the Shan-Chen model [25, 26] for multiphase (MP) and multicomponent (MC) simulations. Although this method has been extended to incorporate a second-neighbour couplings, to improve its isotropy [27, 28]. We simulate multiphase and multicomponent flows using the D2Q9 LBM model (see Fig. 3) [29, 30]. As this method is well established, we provide only the key features for the sake of fixing the notations.

The LBM populations $f_{i,\alpha}(\boldsymbol{x},t)$ correspond to distribution functions at position $\boldsymbol{x}$ and time t for the component α and evolve according to the following equation:

$$f_{i,\alpha}(\boldsymbol{x}+\boldsymbol{e}_i,t+1) - f_{i,\alpha}(\boldsymbol{x},t) = -\frac{1}{\tau_\alpha}\left[f_{i,\alpha}(\boldsymbol{x},t) - f^{eq}_{i,\alpha}(\rho,\boldsymbol{u}^{eq}_\alpha)\right], \tag{3.1}$$

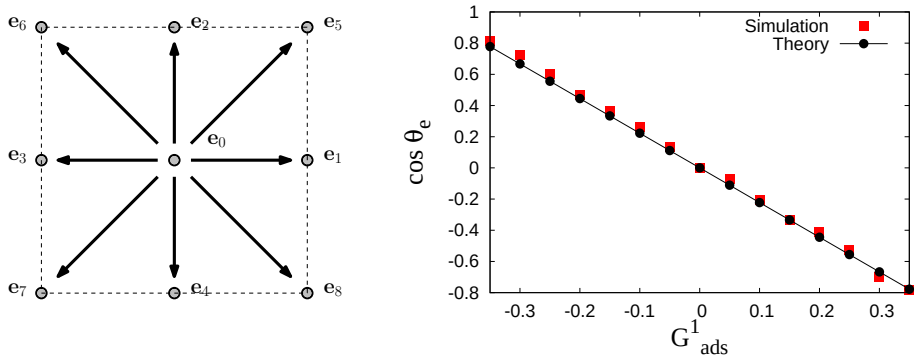

Figure 3: (Left panel) Schematic of the D2Q9 lattice showing the $2d$ spatial discretization (dots) and the nine velocity vectors $\boldsymbol{e}_i$. (Right panel) Comparison of the contact angle obtained from theory, Eq. (3.6), and from our multicomponent LBM simulations. The contact angle from the simulations were obtained by depositing a droplet on a surface with different wetting properties G^1_{ads} and measuring the resulting contact angle.

where the equilibrium distributions, $f^{eq}_{i,\alpha}$, the density, ρ_α, and the momentum, $\rho_\alpha \boldsymbol{u}_\alpha$, for the two components are give by:

$$f_i^{eq,\alpha}(\rho,\mathbf{u}) = \rho_\alpha w_i \left[1+\frac{\boldsymbol{e}_i\cdot\boldsymbol{u}}{c_s^2}+\frac{\boldsymbol{uu}:(\boldsymbol{e}_i\boldsymbol{e}_i-c_s^2\boldsymbol{I})}{2c_s^4}\right], \tag{3.2a}$$

$$\rho_\alpha(\boldsymbol{x},t) = \sum_i f_{i,\alpha}(\boldsymbol{x},t), \tag{3.2b}$$

$$\rho_\alpha \boldsymbol{u}_\alpha(\boldsymbol{x},t) = \sum_i f_{i,\alpha}(\boldsymbol{x},t)\boldsymbol{e}_i\,. \tag{3.2c}$$

Weight w_i in Eq. (3.2), and velocity $\boldsymbol{e}_i$ are the lattice Boltzmann weights and the corresponding lattice speeds [29,30]. These weights are chosen such that it satisfies $\sum_i w_i = 1$ and $\sum_i \boldsymbol{e}_i w_i = 0$ and w_i, corresponding to D2Q9 model, are given by $w_0 = 4/9$, $w_1 = w_2 = w_3 = w_4 = 1/9$, and $w_5 = w_6 = w_7 = w_8 = 1/36$. The total fluid density is $\rho = \sum_\alpha \rho_\alpha$ and the total hydrodynamic velocity is $\boldsymbol{u} = \sum_\alpha u_\alpha \rho_\alpha/\rho$. The effective kinematic viscosity is related to the relaxation time of the different components $\nu = \sum_\alpha c_s^2(\tau_\alpha c_\alpha - 0.5)$ [31], $c_\alpha = \rho_\alpha/\rho$ is the concentration, and $c_s = 1/\sqrt{3}$ is the speed of sound on the lattice. In absence of an external force, each component satisfies the ideal gas equation of state $p = c_s^2\rho$. For multicomponent simulation we are using two distribution functions ($\alpha = 1,2$), whereas for multiphase simulations we restrict ourselves to only one distribution function ($\alpha = 1$).

3.1 Multicomponent model

The multicomponent algorithm is based on a standard Shan-Chen lattice Boltzmann method [25,26,31]. The non-ideal nature of the fluid is introduced by adding an internal

force by shifting the lattice Boltzmann equilibrium velocity as [26,31]:

$$\boldsymbol{u}_\alpha^{eq} = \boldsymbol{u}' + \frac{\tau_\alpha \boldsymbol{F}^\alpha}{\rho_\alpha}, \quad \text{where } \boldsymbol{u}' = \frac{\sum_\alpha \rho_\alpha \boldsymbol{u}_\alpha / \tau_\alpha}{\sum_\alpha \rho_\alpha / \tau_\alpha}. \tag{3.3}$$

For the non-ideal interaction we use a Shan-Chen force [26,31]:

$$\boldsymbol{F}^\alpha = -G\rho_\alpha(\boldsymbol{x}) \sum_{i,\alpha\neq\alpha'} w_i \rho_{\alpha'}(\boldsymbol{x}+\boldsymbol{e}_i)\boldsymbol{e}_i, \tag{3.4}$$

where $\{\alpha,\alpha'\}=\{1,2\}$ indicate the fluid components while the coupling parameter G determines the strength of the interaction and controls the surface tension. This force allows the formation of interface between the different fluid components and the equation of state is modified to $p=c_s^2(\rho_1+\rho_2)+Gc_s^2\rho_1\rho_2$ where the first term correspond to the ideal gas and the second term is the non-ideal part due to the external Shan-Chen force. The surface wetting is introduced by adding an additional force at the wall [32,33]

$$\boldsymbol{F}_{ads}^\alpha = -G_{ads}^\alpha \rho_\alpha(\boldsymbol{x},t) \sum_i w_i s(\boldsymbol{x}+\boldsymbol{e}_i)\boldsymbol{e}_i, \tag{3.5}$$

where $s(\boldsymbol{x}+\boldsymbol{e}_i)=1$ for a wall node and is 0 for a fluid node. The parameter G_{ads}^α can be varied to control the wetting properties of the wall; in all our simulations we have used $G_{ads}^1=-G_{ads}^2$. Huang et al. [32] proposed the following estimate for the contact angle using Young's equation:

$$\cos(\theta_e) = \frac{G_{ads}^1 - G_{ads}^2}{G}. \tag{3.6}$$

The plot in Fig. 3 (right panel) shows the verification of the Eq. (3.6) in our simulations for different values of $G_{ads}^1=-G_{ads}^2$.

3.2 Multiphase model

For the case of a multiphase fluid we have only one fluid component, and only one distribution function *i.e.* $\alpha=1$. The non-ideal nature of the fluid is introduced by adding a self-interaction Shan-Chen force of the form

$$\boldsymbol{F} = -G_{11}\psi(\boldsymbol{x}) \sum_i w_i \psi(\boldsymbol{x}+\boldsymbol{e}_i)\boldsymbol{e}_i, \tag{3.7}$$

where, the pseudo-potential $\psi=[1-\exp(-\rho)]$, see [25]. The equation of state in this case reads $p=c_s^2\rho+G_{11}c_s^2[\psi(\rho)^2]/2$, and high (liquid) and low (vapour) density phase separation is obtained by varying G_{11} [25]. The wetting properties of the surface can be introduced by setting the density at the wall to a value ρ_w $(\rho_2<\rho_w<\rho_1)$. This introduces a modified Shan-Chen force at the wall that leads to a equilibrium contact angle [33,34].

3.3 Limitations and applicability

In this section we discuss some of the issues that emerge when using the LBM to study the problem of a plate dynamically pushed or pulled into a liquid bath. We consider both the multiphase and multicomponent models. To study the problem in all regimes, from the static meniscus to the study of the liquid/gas entrainment, one is interested in small as well as in large values of the capillary number. There are constrains on the possibility to increase the capillary number within LBM: the increase of the wall velocity cannot be pushed too close to the lattice sound speed, the viscosity cannot be increased too much (otherwise the LBM becomes collisionless), the surface tension cannot be decreased too much. For some of these issues partial solutions have been proposed, e.g., the use of multirange models can provide an independent, and thus more flexible, control on the density ratio and surface tension [27], but this involves reverting to more complex LBM methods than the usual first-neighbor Shan-Chen model. Here we show that the multicomponent LBM method is the most suitable tool to investigate the case of small viscosity ratios, while the multiphase is the most suited tool to investigate the case of high viscosity ratio fluids. Our study shows that a single component multiphase model is ideally suited to study film dynamics for high viscosity contrast. Whereas a multicomponent model works better for nearly identical viscosity ratio.

Reducing the surface tension in the multiphase LBM models corresponds to very small density contrast and causes important condensation/evaporation effects [35] at the contact line (see Fig. 4). Partial-wetting conditions may also produce spurious checkerboard oscillations of important amplitude, these oscillations may be controlled by reverting to a Lax-Wendroff streaming scheme [36]. The presence of an open boundary poses important issues for what concerns the stability, the convergence and thus the usability of the method.

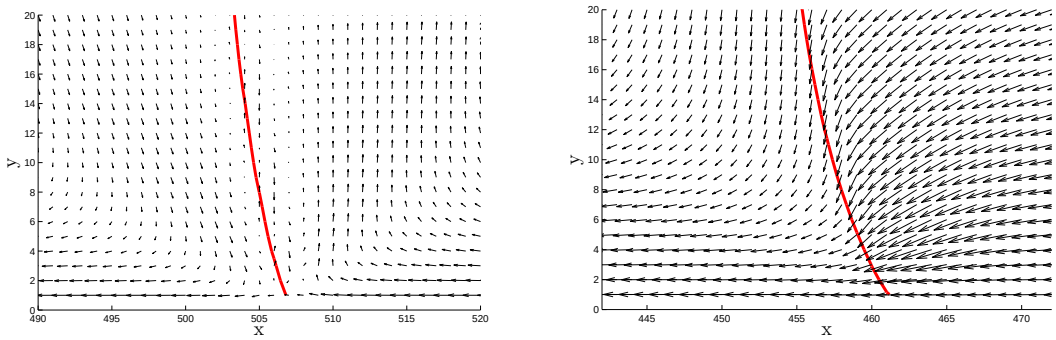

Figure 4: The velocity field (black arrows) and interface position (solid red curve) close to the contact line, for multicomponent LBM simulation (left panel, with $R=1$), and multiphase LBM simulation (right panel, with $R=0.17$). In both cases the plate is moving with velocity $U=-0.01$. The equilibrium contact angle and capillary length for LBM simulations are 62.9^o and $114\ lu$, respectively. Multiphase LBM simulation shows an important mass flux across the interface (right panel), which is absent in the case of the multicomponent LBM simulation (left panel). Base solid blue line is the plate position.

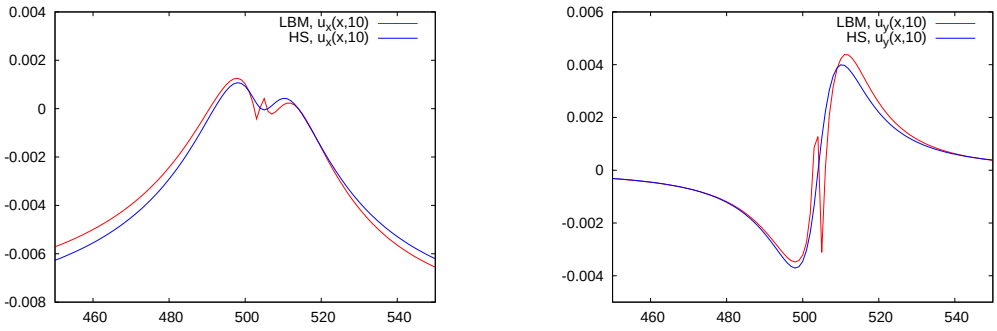

Figure 5: Comparison of velocity $u_x(x,10)$ (left panel), and $u_y(x,10)$ (right panel) between multicomponent LBM, and Huh-Scriven (HS) solution for wedge angle 82^o. The plate velocity and viscosity ratio for both cases are $U=-0.01$, $R=1$ respectively.

A common inconvenience with the Shan-Chen LBM model [25,26] (as well as Cahn-Hilliard models [37]) is the spurious velocity in the vicinity of the interface. These spurious velocities arise due to insufficient isotropy in the calculation of density gradient. Despite these spurious velocities at the interface, the Shan-Chen multiphase and multicomponent LBM models have shown a very good agreement with the sharp interface models [38]. Fig. 5 shows that despite the discontinuity at the interface the velocity field in multicomponent SC LBM is in good agreement with the Huh-Scriven model [12]. The wedge angle in Huh-Scriven model [12] is the angle mage by the straight interface with the plate in the fluid 1.

4 Results

In this section, we present results from both multiphase and multicomponent LBM simulations. For the static case, when the plate velocity $U=0$, we use the Landau solution Eq. (2.1) to benchmark the results from the LBM simulations at varying the channel width, H, and the equilibrium contact angle, θ_e. For this case we also compare the static interface profile for two different boundary conditions and for multiphase and multicomponent simulations.

The numerical study for the moving plate problem is divided into two parts: *i.e.*, $U>0$, the LLD problem, and $U<0$, the plunging plate problem. The steady state interface profile obtained from the multicomponent LBM simulations are compared with the interface profile obtained from lubrication theory [24].

The complete list of LBM simulations for plunging plate problem are reported in Table 1 while the parameters corresponding to the LLD problem are shown in Table 2. The capillary length and the domain length, L, have been kept fixed for all the results presented here.

The capillary length for multicomponent simulations is obtained using $l_c=\sqrt{\gamma_{12}/(\rho_1 g)}$, whereas for the multiphase simulations the capillary length has been obtained using

Table 1: List of multicomponent LBM simulations for the plunging plate problem. For these tests following parameters remains unchanged: Length of the channel $L = 640$, interaction parameter $G = -0.9$, $\rho_1 = 0.06$, ρ_2=2.00 are the low and high densities, respectively, for both fluid components, relaxation parameters $\tau_1 = \tau_2 = 1$, body force $g = 6.82 \times 10^{-6}$ and the density difference at bottom boundary $\Delta\rho = 0.02$. The physical parameters for these simulations are: $l_c = 114.73$, $\gamma_{21} = 0.183$, dynamic viscosities $\mu_1 = \mu_2 = 0.34$, and the viscosity ratio $R = \mu_2/\mu_1 = 1$.

	H	θ_e (degree)	U
PP0-128	128	62.2	0.0
PP0-256	256	62.2	0.0
PP0-384	384	62.2	0.0
PP0-512	512	41.3, 52.3, 62.2, 70.3, 77.5, 102.5, 109.7, 117.8	0.0
PP0-1024	1024	62.2	0.0
PP1-128	128	62.2	-0.005
PP1-256	256	62.2	-0.005
PP1-384	384	62.2	-0.005
PP1-512	512	62.2	-0.005
PP1-1024	1024	62.2	-0.005
PP2-128	128	62.2	-0.01
PP2-256	256	62.2	-0.01
PP2-384	384	62.2	-0.01
PP2-512	512	62.2	-0.01
PP2-1024	1024	62.2	-0.01

Table 2: List of multicomponent LBM simulation for the LLD problem. We choose the parameters L, ρ_1, ρ_2, G, τ_1, τ_2, g, l_c, γ_{21}, μ_1, μ_2, and R same as given in Table 1, except $\Delta\rho$ for these test is 0.008.

	H	θ_e (degree)	U
LL0-128	128	62.2	0.001
LL0-256	256	62.2	0.001
LL0-384	384	62.2	0.001
LL0-512	512	62.2	0.001
LL1-128	128	62.2	0.005
LL1-256	256	62.2	0.005
LL1-384	384	62.2	0.005
LL1-512	512	62.2	0.005

$l_c = \sqrt{\gamma_{12}/((\rho_1 - \rho_2)g)}$. The surface tension values for both multiphase and multicomponent simulations are obtained using the Laplace test [25], the relaxation parameter for the multiphase LBM simulations presented in this manuscript is one ($\tau = 1$). The two relaxation parameters in the multicomponent LBM simulation are identical and equal to one ($\tau_1 = \tau_2 = 1$). A detailed study of LBM results based on different values of relaxation parameters is beyond the scope of this paper.

4.1 Static meniscus

As a first step we proceed with the validation of the LBM for the static case. We focus on both open and wall bounded baths and on both the multiphase and multicomponent methods. In the case of the multiphase model a body force g applied everywhere. A side effect of the multiphase LBM is that the dynamic viscosity is proportional to the density and therefore the method is restricted to compute film dynamics between two fluids with high density ratio (e.g. water in air). For a multicomponent fluid, instead, the density ratio cannot be easily pushed to large values, while the viscosity ratio can be taken easily to be of order unity. Thus it is necessary to devise a different procedure to give rise to the static meniscus.

For the multicomponent LBM simulation our approach consists in keeping the densities of the two component equal, therefore we apply pressure and gravity only on one fluid component, ρ_1. In this test we validate this assumption by comparing the multicomponent simulation with the multiphase LBM simulation where we apply pressure and gravity on both phases. This approach has been validated against the multiphase case, see Fig. 6 (left panel). The simulation parameters for multiphase simulation were: system size $L\times H=640\times 256$, $G_{11}=-6.0$, $\rho_l=2.65$, $\rho_v=0.075$, $\tau=1$, $\nu=0.1666$, $\gamma_{21}=0.1444$, body force $g=4.271\times 10^{-6}$, density difference at bottom boundary $\Delta\rho=0.027$, $l_c=114.73$, and the static contact angle θ_e=62.2^o. We use multicomponent simulation PP0-256 to compare the static interface profile. The result for this test (see Fig. (6) (left panel)), shows a very good agreement between the two approaches. This indicates that the both multiphase and multicomponent LBM can be employed to study capillarity effects. We stress here that the combined possibility to use either a multiphase or a multicomponent LBM is key to investigate the meniscus dynamics at both large or small values for the viscosity ratios.

In order to investigate the effect of boundary conditions at the right boundary (see Fig. 1), we are using open and wall boundary conditions on right boundary. In order to implement the open boundary condition, we initialize the unknown incoming the populations to the equilibrium distribution $f^{eq}_{i,\alpha}(\rho,\mathbf{u})$. Since the calculation of the equilibrium distribution function requires the information of the density and velocity, we use the values of density and velocity from the lattice nodes adjacent to the right boundary. The wall boundary condition on right boundary is the standard mid-grid bounce back boundary condition [29]. The Shan-Chen force which has been used to model the contact angle on the wall (left boundary) has been switched off the for right boundary.

The first observation, using open boundaries, is that this boundary condition is very sensitive to the initialization and its convergence times are extremely long, probably due a minor dissipation, as compared to no-slip boundary condition. Once the interface reaches a stationary state we compare the profiles obtained with the two boundary conditions. As shown in Fig. 6 (right panel) the result from the two simulations are in good agreement with each other as well as with Landau's solution, at least close enough to the contact line.

To further validate the multicomponent LBM for the study of the static meniscus, we

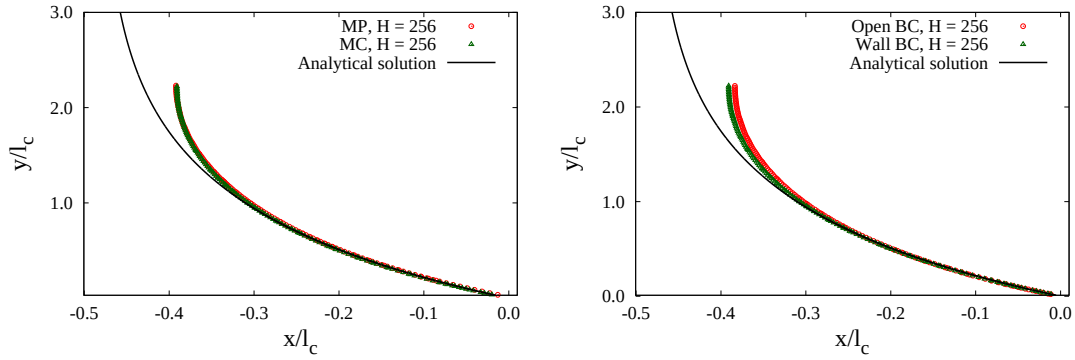

Figure 6: A comparison of interface profiles for plate velocity $U=0$. (Left panel) Comparison of the analytical solution Eq. (2.1), and multicomponent and multiphase simulations for the no-slip boundary conditions at the right boundary. (Right panel) Comparison of analytical solution Eq. (2.1) and multicomponent LBM simulations for two different boundary conditions on the right boundary.

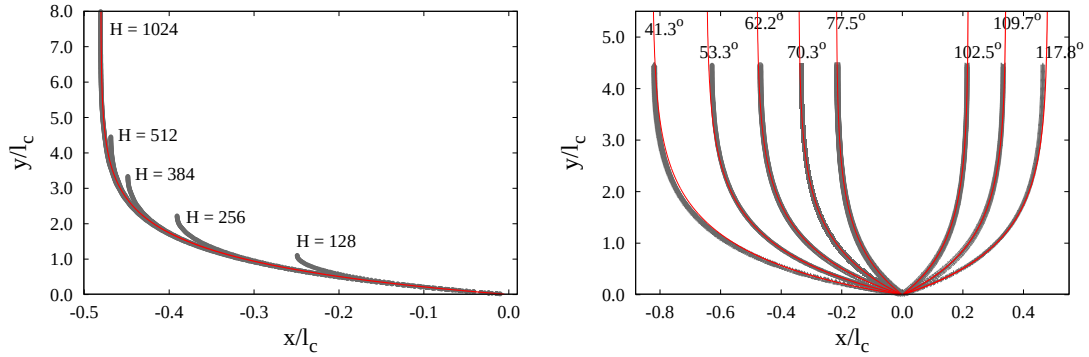

Figure 7: (Left panel) Comparison of the analytical solution Eq. (2.1) (solid red curve), and LBM solution for different channel width H for $U=0$. (Right panel) Validation of the LBM solution for different static contact angles against the analytical solution Eq. (2.1) (solid red curve).

investigate systems with different bath width, H (with respect to the capillary length, l_c) and with different wall wettability. We compare all these cases against Landau's solution Eq. (2.1). The parameters employed for the multicomponent LBM are reported in Table 1 (PP0-128,$\cdots$,PP0-1024). As already explained the body force g and the pressure jump counteracting the hydrostatic pressure are only applied on one fluid component (ρ_1). These simulations are done using mid-grid bounce back boundary conditions [29] at both left and right walls; the wetting condition is used on the plate wall. The result for the test with different bath widths H are shown in Fig. 7 (left panel), where lengths are expressed in units of the l_c and the contact line position is shifted to pass through the origin. We notice that close to the contact line the solution is always in good agreement with the analytical one, but only for larger system sizes the accuracy extends up to well outside the static meniscus. In particular the reference simulation with width as large as $H=1024$

is matching the analytic solution till well inside the bath. The second validation involves the multicomponent LBM simulation (PP0-512) with different static contact angles $\theta_e = 41.3^o, \cdots, 117.8^o$ and is reported in Fig. 7 (right panel). The LBM results for these tests are in good agreement with Landau's solution Eq. (2.1).

4.2 Results for moving plate (dry regime)

In this section we discuss the case when the plate is either pulled $(U>0)$ or plunged $(U<0)$ into a liquid bath of density ρ_1. For small plate velocity, as already discussed, one does not expect the formation of a liquid or gas film, we refer to this regime as to the dry regime. We report two sets of simulations for the study of interface profile for the case of moving plate.

In first set of simulations we show the multicomponent LBM for simulations for the LLD problem $(U>0)$, and compare these results against the lubrication theory approximation [24]. Parameters corresponding to this set of LBM simulations are shown in the Table 2. Fig. 8 (left panel) shows the result for $Ca=0.0187$ and different H, and Fig. 8 (right panel) shows the result for $Ca=0.0938$ and different H. The multicomponent LBM results are in good agreement, for higher H, with the corresponding result from lubrication theory based model using a value $l_s = 10^{-3}$ for the slip length. We are using wall boundary condition on right boundary for these simulations.

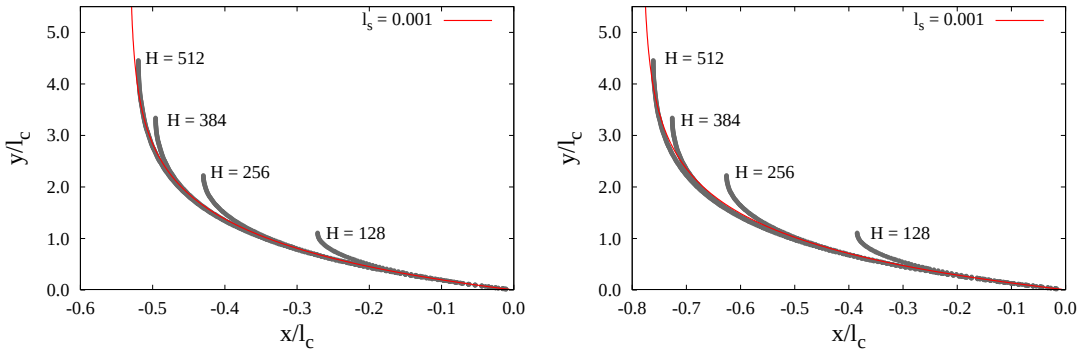

Figure 8: (Left panel) Comparison of the steady state interface profile for plate velocity $U=0.001$ between lubrication theory (solid red curve) and the multicomponent LBM simulations for different H. (Right panel) Comparison of the steady state interface profiles for the case of plate velocity $U=0.005$ between the lubrication theory (solid red curve) and the multicomponent LBM simulations. For these simulation $R=1$, and $\theta_e=62.9^o$. A detailed list of parameters for these simulations is shown in Table 2.

One can estimate a-priory that the slip length, l_s, for LBM will be in the order of one grid point(in lattice units). For a quantitative comparison between LBM and LT one need to tune the definition of the slip length in the two cases. This was done for one particular wall velocity (see Fig. 9, left panel). This value of l_s for LT was then used for quantitative matching for all Ca values.

In Fig. 9 (left panel) we report the steady state interface profile for the case of a plung-

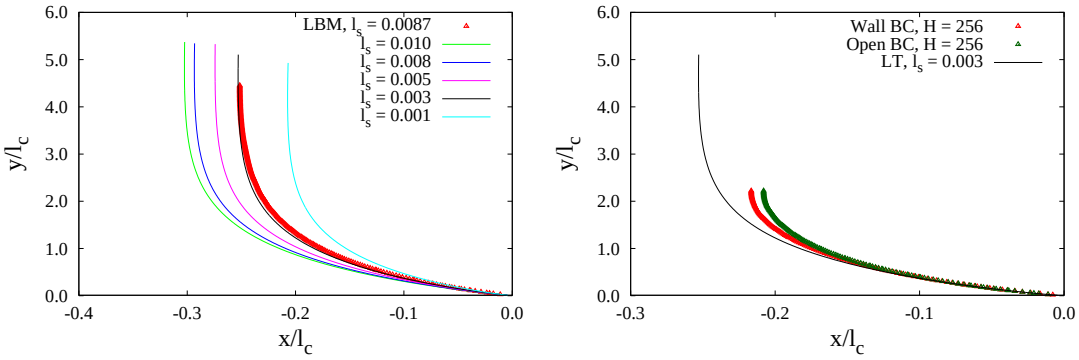

Figure 9: (Left panel) Comparison of the steady state interface profile for plate velocity $U=-0.005$ between lubrication theory for different l_s and multicomponent LBM simulation (solid red curve). (Right panel) Comparison of steady state interface profile at plate velocity $U=-0.005$ for different boundary conditions. For these simulation $R=1$, and $\theta_e=62.9^o$.

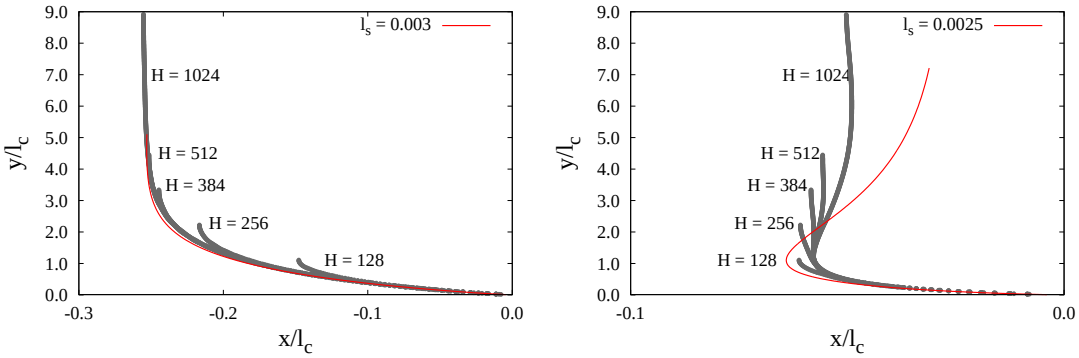

Figure 10: (Left panel) Comparison between lubrication theory (solid red curve) and multicomponent LBM simulations at $U=-0.005$ for varying H. (Right panel) Same as in the left panel but for $U=-0.01$. For these simulation $R=1$, and $\theta_e=62.9^o$.

ing plate problem ($U<0$) (see Fig. 1(right panel)) for a small capillary number Ca=0.0187. To compare against the solution from lubrication theory we need to estimate the slip length. In the case of the LBM we can estimate this as being in the order of one lattice site; the agreement with lubrication theory is quite good once the slip length is better tuned (roughly a factor 3 with respect to our estimate). In Fig. 9 (right panel) we show that for this particular capillary number the shape of the interface does not seems to be sensitive to the boundary conditions used on the right boundary of bath (see Fig. 1). In Fig. 10 (left panel) it is further shown that the solution obtained converges quite rapidly to the solution for an infinite bath, similar to what was found for the case of a static wall. When the capillary numbers is increased, see Fig. 10 (right panel), we not only observe important deviations from the lubrication theory solution but also important dependence on the H.

5 Conclusions

The behavior of a fluid at the three-phases contact, e.g. amongst a solid a liquid and its vapor, has been studied at length and still poses many interesting and fundamental scientific questions. Here we discussed the possibility to employ simple and standard implementations of the Lattice Boltzmann method for multiple phases or components in order to study the problem under both static and dynamic (i.e. moving wall) conditions. We showed that the multicomponent LBM can effectively replace the multiphase modeling by applying the gravitational field, along with balancing hydrostatic pressure at the bottom, on only one fluid component. The multicomponent LBM is less sensitive to condensation and evaporation phenomena at the contact line and thus outperforms the multiphase method for the case of small viscosity ratio between the two fluids.

Outlook on entrainment regime

For the static meniscus case we observe a rather fast convergence towards the analytic solution at increasing the ratio between the bath width and the capillary length; capillarity effects due to change in the contact angle were quantitatively reproduced. In the case of moving wall we observe agreement with lubrication theory solutions only at small capillary numbers. For larger capillary numbers we observe a rather strong dependency on the capillary length, presumably due to a stronger influence of the large scale flow which can occur due to presence of the confining bath wall.

Though this was out of the scope of the present study, it may be possible to extend and improve on these results by reverting to more sophisticated (and computationally expensive) implementation of the LBM. As an example multirange interaction can provide extended flexibility in the control of the physical parameters.

The proposed LBM can be used to study more complex boundary conditions, transient flow regime and film entrainment. Results in this direction will be reported elsewhere [39].

Acknowledgments

The author acknowledge discussions with Bruno Andreotti, Jacco Snoijer and Tak Shing Chan. This work has been funded by FOM (Foundation for Fundamental Research on Matter).

References

[1] P. G. De Gennes, Rev. Mod. Phys. 57, 827-863 (1985).
[2] T. D. Blake, J. Colloid Interface Sci. 299, 1-13 (2006).
[3] A. Oron, S. H. Davis & G. Bankoff, Rev. Mod. Phys. 69, 931-980 (1997).
[4] J. Eggers, Phys. Fluids 17, 082106 (2005).
[5] M. T. Ghannum & M. N. Esmail,AIChe J. 39, 361-365 (1993).

[6] R. Golestanian & E. Raphael, Phys. Rev. E 64, 031601 (2001);
[7] L. M. Hocking, J. Appl. Maths. 12, 195-208 (2001).
[8] J. H. Snoeijer, J. Ziegler, B. Andreotti, M. Fermigier & J. Eggers, Phys. Rev. Lett. 100, 244502 (2008)
[9] J. H. Snoeijer, G. Delon, M. Fermigier, & B. Andreotti, Phys. Rev. Lett. 96, 174504 (2006).
[10] L. D. Landau & B. V. Levich, Acta Physicochim. URSS 17, 42 (1942).
[11] B. V. Derjaguin, Acta Physicochim URSS 20, 349 (1943).
[12] C. Huh & L. Scriven, J. Colloid Interface Sci. 35, 85-101 (1971).
[13] P. G. De Gennes, Colloid Polym. Sci. 264, 463 (1986).
[14] J. A. Tallmadge, AIChE J. 16, 925 (1970).
[15] B. M. Deryagin & S. M. Levi, Film Coating Theory, Focal Press, London, (1964).
[16] A. de Ryck & D. Quéré, J. Colloid Interface Sci. 203, 278 (1998).
[17] O. O. Ramdane & D. Quéré, Langmuir 13, 2911 (1997).
[18] J. Eggers, Phys. Rev. Lett. 93, 094502 (2004).
[19] F. P. Bretherton, J. Fluid Mech., 10, 166-188 (1961).
[20] T. Young Phil. Trans. R. Soc. Lond 95, 65-87 (1805).
[21] P. G. De Gennes, Capillarity and Wetting Phenomena: Drops, Bubbles, Pearls, Waves, Springer, New York (2003).
[22] O. V. Voinov, Fluid Dyn. Engl. Transl. 11, 714 (1976).
[23] R. G. Cox, J. Fluid Mech. 168, 169 (1986).
[24] A. Marchand, T. S. Chan, J. H. Snoeijer & B. Andreotti, arXiv:1110.5274, (2011); and private communication.
[25] X. Shan & H. Chen, Phys. Rev. E 47, 1815-1819 (1993).
[26] X. Shan & H. Chen, Phys. Rev. E 49, 2941-2948 (1994).
[27] M. Sbragaglia, R. Benzi, L. Biferale, S. Succi, K. Sugiyama & F. Toschi, Phys. Rev. E 75, 026702 (2007)
[28] X. Shan, Phys. Rev. E 73, 047701 (2006).
[29] S. Succi, The Lattice Boltzmann Equation for Fluid Dynamics and Beyond, Oxford University Press (2001).
[30] D. A. Wolf-Gladrow, Lattice-Gas Cellular Automata and Lattice Boltzmann Models - An Introduction, Springer-Verlag Berlin Heidelberg (2005).
[31] X. Shan & G. Doolen, J. Stat. Phys. 81 379 (1995).
[32] H. Huang, D. T. Throne, M. G. Schaap & M. C. Sukop, Phys. Rev. E 76, 066701 (2007).
[33] R. Benzi, L. Biferale, M. Sbragaglia, S. Succi & F. Toschi, Phys. Rev. E 74, 021509 (2006).
[34] M. Sbragaglia, R. Benzi, L. Biferale, S. Succi & F. Toschi, Phys. Rev. Lett. 97, 204503 (2006).
[35] A. J. Briant, A. J. Wagner, & J. M. Yeomans, Phys. Rev. E 69, 031602 (2004).
[36] Z. Guo, B. Shi & C. Zheng, Phil. Trans. R. Soc. A 369, 2283 (2011).
[37] L. Scarbolo, D. Molin, P. Perlekar, M. Sbragaglia, A. Soldati & F. Toschi, J. Comput. Phys., submitted (2011).
[38] M. Sbragaglia, K. Sugiyama & L. Biferale, J. Fluid Mech. 614, 471 (2008).
[39] S. Srivastava, L. Biferale, P. Perlekar, & M. Sbragaglia, in preparation (2011).